Impact of sonication on the rheological and colloidal properties of highly concentrated cellulose nanocrystal suspensions

Erwan Gicquel, Julien Bras, Candice Rey, Jean-Luc Putaux, Frédéric Pignon, Bruno Jean, Céline Martin

Impact of sonication on the rheological and colloidal properties of highly concentrated cellulose nanocrystal suspensions

Erwan GICQUEL[1], Julien BRAS[1,4], Candice REY[2], Jean-Luc PUTAUX[3], Frédéric PIGNON[2], Bruno JEAN[3], Céline MARTIN[1#]

[1] *Univ. Grenoble Alpes, CNRS, Grenoble INP*, LGP2, F-38000 Grenoble, France*

[2] *Univ. Grenoble Alpes, CNRS, LRP, F-38000 Grenoble, France*

[3] *Univ. Grenoble Alpes, CNRS, CERMAV, 38000 Grenoble, France*

[4] *Institut Universitaire de France, F-75000 Paris, France*

(* Institute of Engineering Univ. Grenoble Alpes)

_____

#Contact E-mail : celine.martin@grenoble-inp.fr

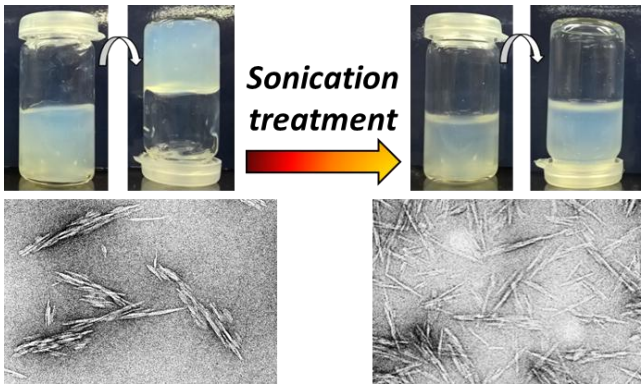

ABSTRACT

The effect of sonication on a highly concentrated commercial suspension of cellulose nanocrystals (CNCs) and the resulting rheological properties have been investigated. Rheology and structural analysis techniques (atomic force microscopy, small-angle X-ray scattering, transmission electron microscopy and dynamic light scattering) were used to characterize the CNC suspension before and after sonication as a function of concentration. The highly concentrated CNC suspension, which does not contain aggregates, as shown by AFM and TEM imaging, turns from a "gel" form into a "liquid" form after a sonication treatment. The self-organization properties of as-prepared and sonicated suspensions were compared by the determination of their phase diagrams and flow rheology was performed to understand the viscosity behavior as a function of concentration for both systems. Sonication induced a decrease of the inter-particular distance, a strong decrease of the viscosity and remarkable changes in the liquid crystalline behavior, while sonicated and non-sonicated suspensions were stable over time. These effects can be attributed to a decrease in the aspect ratio of the suspended particles, which varies from a high value before sonication due to the presence of elongated bundles to a lower value after sonication that promotes individualization.

Keywords: *Cellulose nanocrystals (CNCs), rheology, sonication, self-organization, aspect ratio*

Introduction

As biodegradable, renewable, non-toxic and high-performance nanomaterials, cellulose nanocrystals (CNCs) have evolved from a laboratory curiosity to a technical material, which has attracted industrial attention. These rod-like nanoparticles initially reported in the 1950's are commonly obtained by acid hydrolysis of cellulosic material at about 2-5% solid content (Rånby, 1951; Revol et al., 1992). CNCs are now produced in several countries at pilot or commercial scale by various companies since the 2010's (Reid et al., 2017). Their size, shape and surface properties both depend on the origin of the cellulose source and on the hydrolysis conditions (Beck-Candanedo et al., 2005; Bras et al., 2011; García et al., 2016). Owing to their specific physical properties and high aspect ratio, CNCs are used in the development of several applications in various fields (Tang et al., 2017) such as the biomedical domain (Jorfi and Foster, 2015; Lin and Dufresne, 2014; Sunasee et al., 2016), environmentally friendly nanocomposites (Mariano et al., 2014; Oksman et al., 2014; Siqueira et al., 2010) or the paper coating industry (Gicquel et al., 2017; Hoeng et al., 2017). In each case, the rheological properties and their variation with concentration play a major role. Recently, new processes have been proposed to favor industrialization and new grade delivery. Highly concentrated suspensions (up to 11 wt%) are now commercially available (Reid et al., 2017). This study focuses on this grade.

As other colloidal rods like DNA fragments (Hamley, 2010), viruses (Watson, 1954), metal oxides (Zhang et al., 2005) or chitin nanocrystals (Revol et al., 1992), CNC suspensions exhibit very interesting self-organization properties: above a critical concentration, the suspension phase-separates into an upper isotropic phase and a lower anisotropic chiral nematic phase (Revol et al., 1992, 1994). The formation of this phase can be explained by Onsager's theory (Onsager, 1949), which predicts the critical transition density for very high aspect ratio hard rods. This theory was further refined to take into account smaller aspect ratios, polydispersity and most importantly electrostatic interactions (Araki and Kuga, 2001; Dong and Gray, 1997; Lee, 1987). The dimensions, aspect ratio, surface charge density and surface chemistry greatly influence the phase separation behavior and the characteristics of the cholesteric liquid-crystalline phase (Abitbol et al., 2018; Azzam et al., 2016; Lagerwall et al., 2014; Revol et al., 1994; Shafiei-Sabet et al., 2014).

The rheological behavior of aqueous CNC suspensions stands as a major concern of high application-relevance and different studies over the past 10 years were dedicated to its

comprehensive understanding (Bercea and Navard, 2000; Liu et al., 2011a, 2011b; Lu et al., 2014; Shafiei-Sabet et al., 2012, 2014; Ureña-Benavides et al., 2011; Xu et al., 2017a, 2017b). One of the important reported results is the effect of concentration and the related position in the phase diagram. While isotropic suspensions behave like classical polymer solutions, the viscosity profile as a function of shear rate observed for liquid crystalline and biphasic CNC suspensions decomposes into three distinct regions (Bercea and Navard, 2000; Shafiei-Sabet et al., 2012). Namely, at low shear rate, a first shear-thinning region due to the alignment of chiral nematic domains is observed. At intermediate shear rates, a plateau with constant viscosity is observed. It is corresponded to the alignment of all chiral nematic domains in the flow direction. Finally, at high shear rate, chiral domains are disrupted and all CNCs align in the flow, leading to a second shear-thinning region.

Nonetheless, most studies have focused on low concentration suspensions or at least have used such suspensions as starting material. Furthermore, limited information exists on the relationship between macroscopic rheological properties and the microscopic structure of CNCs suspensions whatever the concentration is. A few works involve rheology coupled with scattering techniques such as small-angle neutron, small-angle X-ray and light scattering (SANS, SAXS, and SALS, respectively) to characterize the orientation and morphology of CNCs under flow (Ebeling et al., 1999; Orts et al., 1998; Schütz et al., 2015; Xu et al., 2017a). Orts et al. (Orts et al., 1998) showed that CNC rods are oriented parallel to shear flows with increasing shear rate.

Ultrasound treatment (also called sonication) is ordinarily used at the end of the process of creation of CNCs and also to disperse CNC aggregates in dilute suspension (Beuguel et al., 2018; Csiszar et al., 2016; Dong et al., 1996), which generally causes a decrease in viscosity in dilute conditions (Beuguel et al., 2018; Dong et al., 1998; Marchessault et al., 1961; Shafiei-Sabet et al., 2012). This viscosity variation is important and, to our knowledge, the effect of sonication on the rheological behavior and microstructure (like inter-particle distance) of highly concentrated CNC suspension has not been studied in details.

Beck et al. (Beck et al., 2010) evaluated the impact of ultrasound energy on CNCs in dilute conditions (~3 wt%) to prepare colored solid films and control their optical properties. The authors found that the chiral nematic pitch in the CNC films increased with increasing sonication energy input resulting in a change in the film color. Shafiei-Sabet et al. (Shafiei-Sabet et al., 2012) investigated the effects of concentration, temperature and sonication on the

microstructure and rheological behavior of aqueous CNCs suspension. They prepared suspensions from freeze-dried CNCs and reached a maximum concentration of ~7 wt%. They found that the minimum amount of sonication necessary to disperse aggregates was 1000 $J \cdot g^{-1}$ whatever the concentration. Nonetheless, they did not observe any cholesteric phase formation before sonication. Beuguel et al. (Beuguel et al., 2018) investigated the impact of ultrasonication on dilute CNCs suspension (< 5wt.%) after spray- and freeze-drying process. They explained that sonication break aggregates and release ions/water but the energy generated by sonication was not sufficient to desulfate CNCs. Csiszar et al. (Csiszar et al., 2016) evaluated the impact of sonication time at the end of the preparation process on the CNCs size and on the transparency of CNCs films. Honorato-Rios et al. (Honorato-Rios et al., 2018) recently examined the impact of salt on liquid crystal behavior after sonication of CNCs suspensions over a broad range of concentration.

In the present study, never dried highly concentrated CNC suspensions have been submitted to a sonication treatment which induced a clear change in the rheological behavior (**Fig. 1)**. The non-sonicated suspension existed in a stable gel-like state, while after sonication, the suspension was liquid and able to flow when the vial was turned upside down. Besides, cholesteric domains could form before the sonication treatment (**Support information S1**). In order to highlight the origin of this phenomenon, we have studied the impact of sonication on the morphology, self-organization properties and rheological behavior of CNCs using suspensions with concentrations spanning over a wide range (from 1 to 12 wt%).

This article is part of the Ph.D. thesis "*Development of stimuli-responsive cellulose nanocrystals hydrogels for smart applications*" by Erwan GICQUEL (Gicquel, 2017).

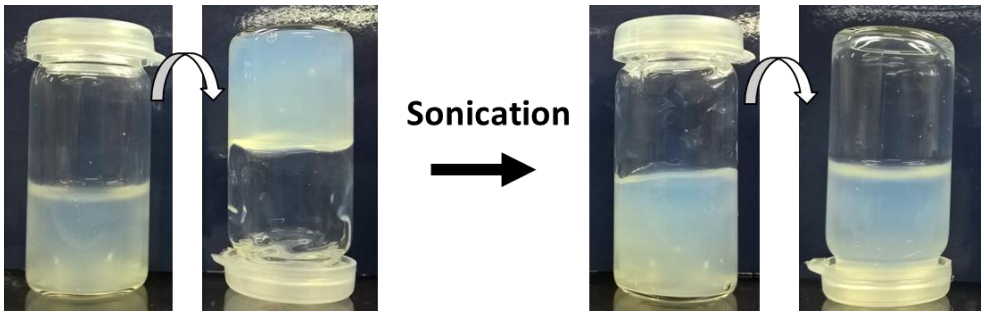

Fig. 1 Effect of sonication (5000 J/g_{CNC}) on the flow properties of a 12 wt% CNC suspension.

1. Materials and Methods

1.1. Materials

The commercial cellulose nanocrystals (CNCs) used in this study were purchased from UMaine Development Center (Forest Products Laboratory, USA) and used as received. These CNCs have been produced from wood pulp using sulfuric acid hydrolysis. The colloidal suspension was never freeze-dried and the dry matter content determined with a moisture analyzer (Ohaus® MB-35, Sigma-Aldrich, USA) was ~12 wt%. The sulfur content of the suspension is 1 wt.% as determined in recent article (Honorato-Rios et al., 2018; Xu et al., 2017b).

1.2. CNC suspension characterization

Atomic force microscopy (AFM): CNCs were imaged using AFM (Dimension icon®, Bruker, USA). All suspensions were previously diluted to 10^{-4} wt% and a drop of 0.2 mL was deposited onto a freshly cleaved mica plate. Samples were dried overnight at room conditions. The samples were characterized in tapping mode using a silica coated cantilever (OTESPA® 300 kHz - 42 N/m, Bruker, USA). Scans of 10x10 µm² and 3.3x3.3 µm² were performed to analyze the dimensions of CNCs. At least 4 images per sample were obtained. In order to extract the length and width dimensions, measurements of about 200 particles were performed by using the ImageJ software to obtain a representative average size.

Transmission electron microscopy (TEM): Drops of about 0.001 %wt CNC suspensions were deposited onto glow-discharged carbon-coated TEM grids. After 2 min, the liquid in excess was absorbed with filter paper, and prior to drying, a drop of Uranyless negative stain (Delta Microscopies, France) was deposited. After 2 min, the solution in excess was blotted and the grid was air-dried. The specimens were observed using a Philips CM200 microscope (FEI, USA) operating at 200 kV. The images were recorded with a TVIPS TemCam F216 digital camera. In order to measure the length of the particles. About 150 particles were measured from the images using ImageJ and calculate a representative average size.

Dynamic light scattering (DLS): Dynamic light scattering measurements were performed on CNC suspensions using a Vasco® I DLS apparatus (Cordouan Technologies). Samples were diluted in deionized water to 10^{-2} wt% and the conductivity was adjusted to 500 $\mu S \cdot cm^{-1}$ by addition of a NaCl solution. The hydrodynamic diameter (z*) and polydispersity index (PDI)

were calculated using cumulant analysis. For each sample, the final values represent an average of at least 3 acquisitions with 10 measurements.

1.3. Small-angle X-ray scattering (SAXS)

SAXS measurements were carried out at the ID02 TRUSAXS beamline of the European Synchrotron Radiation Facility (ESRF, Grenoble, France). A monochromatic X-ray beam at a wavelength of 0.995 Å was used. Scattered intensities were recorded on a two-dimensional CCD detector at sample-detector distances of 2 and 10 m in order to cover a q domain ranging from 10^{-3} to 10^{-1} $Å^{-1}$. Samples were placed in flow-through cells (diameter 1.7 mm), and were left at rest for 5 min before acquisition. The background scattering of pure water and the capillary were subtracted prior to radial integration.

Particle size: The scattering intensity distribution $I(q)$ as a function of the scattering vector Q was obtained by radially integrating the two-dimensional (2D) scattering patterns. The particle length, width and thickness *(a, b* and *c*, respectively) were extracted from the fitting of the scattering profile with the form factor of a parallelepiped using the SasView® 4.0.1 modeling software.

Interparticle distance: A Kratky plot (corresponding to $q^2 \cdot I(q)$ *vs* q) analysis was performed to measure the average interparticular distance, *d*. In this representation: $d = 2\pi/q_{peak}$, where q_{peak} is the position of the scattered intensity maximum.

1.4. CNC dispersion and dilution

Non-sonicated suspensions: To obtain a homogeneous and well-dispersed suspension, the desired weight concentration of the CNC suspension was diluted with deionized water (pH = 6) with fixed ionic strength (18 mM or 1300 $\mu s \cdot cm^{-1}$ obtained with addition of NaCl). Then, this suspension was magnetically stirred for at least 2 h.

Sonicated suspensions: The dilution was identical to that of non-sonicated dispersions. These suspensions were exposed to a dispersive energy of 5 kJ per g of dry CNCs using a 250 W sonication probe (Sonifier S-250A, Branson, USA) at 50% of maximum energy. To prevent thermal degradation of the CNCs during sonication, the temperature of the sample was control to keep room temperature without excess heating thanks to a container with ice.

Mechanically-homogenized dispersions: The dilution was identical to that of non-sonicated dispersions. The suspensions were then mechanically mixed with an Ultra-turrax (IKA T25 digital) at a speed of about 5000 rpm.

1.5. CNC suspension concentration

Sonicated suspensions: The starting solution at 12 wt% was sonicated at 5 kJ per g of CNCs using a 250 W sonication probe (Sonifier S-250A, Branson, USA). Then, the suspension was concentrated with an EMD Millipore Amicon® bio-separation stirred cell (Merck KGaA, Darmstadt, Germany). The highest concentration that was reached was 17.6 wt%.

1.6. CNC phase diagram

Non-sonicated suspensions: Samples from 1 to 12 wt% (with 1 wt% steps) were poured into 5 mL sealed glass vials and allowed to rest for at least 10 days at room temperature. These vials were observed between crossed-polars and pictures were recorded using a digital camera. The isotropic/anisotropic phase ratio was obtained from the height of each phase measured on these images.

Sonicated suspensions: The protocol was identical to that used for non-sonicated suspensions to prepare samples from 1 to 17.6 wt% (with 1 wt% steps).

1.7. Rheological experiments on CNC suspensions

The rheology behavior of the aqueous CNC suspensions under shear was studied using two different rotational rheometers: the Physica MCR 301 (Anton-Paar, Austria) and DHR3 (TA Instruments, New Castle, DE) instruments. The tests were carried out at a temperature of 20 °C. Shearing tests were performed with a cone-plate configuration (diameter of 50 mm and angle of 1° for MCR 301 and diameter of 65 mm and angle of 2° for DHR3). The atmosphere around the sample was saturated with water to avoid evaporation during the measurement. To control the initial state of each sample, a constant shear rate was applied. The transient response under shear was recorded until steady conditions were obtained. Steady shear viscosity versus shear rate curves were generated for each sample from a shear rate of 0.01 to 1000 s^{-1}. The time required to reach steady conditions was decreased with increasing shear rate. Oscillatory measurements were also performed to collect the relaxation time and the elastic behavior of each sample. The percent strain used was inside the linear viscoelastic region (LVE) as determined by performing strain sweep experiments at a frequency of 1 Hz. Then the percent strain (obtained in the LVE) was fixed and oscillation sweep experiments

were performed. The frequency used for oscillatory measurements was also inside the LVE.. These two values were fixed to obtain the storage modulus (G', Pa) and the loss modulus (G'', Pa) before and after a strong shear deformation (up to 100 s^{-1}).

2. Results & Discussions

2.1. CNC morphology

AFM and TEM images of CNC particles before and after sonication are shown in **Fig. 2**. These data reveal changes in morphology, size and size distribution upon the sonication treatment. Before sonication, the particles clearly exhibit a composite aspect and are formed of the lateral association of elementary rod-like crystallites (**Fig. 2b** and **c**). These particles are not aggregated but images reveal elongated objects composed of laterally associated elementary crystallites. In a particle, the constituting crystallites are all parallel and their number is estimated to range between 4 and 20 (determined from TEM images). The average length was 217 ± 42 nm, measured from AFM and TEM images. The average height, determined from the AFM images, was 10 ± 5 nm (**Fig. 2a**), a value which is rather close to the lateral size of the constituting crystallites and suggests that the particles have a lamellar shape.

After sonication, the particles appear to be smaller both in length and width, and the number of constituting crystallites has decreased to a few units (about 1 to 4) (**Fig. 2e** and **2f**). The average length was 150 ± 30 nm (AFM & TEM images) and the CNCs' height was still 10 ± 5 nm (**Fig. 2d**). The values after sonication of the CNCs are in line with the literature data on CNCs from wood pulp (Habibi et al., 2010; Lagerwall et al., 2014; Shafiei-Sabet et al., 2012). Such a composite morphology of CNCs from different botanical sources has already been described by other authors (Chauve et al., 2014; Elazzouzi-Hafraoui et al., 2008). It is considered to originate from the strong lateral association of cellulose microfibrils after drying of the raw material. The strong acid hydrolysis and subsequent sonication treatments during the process of fabrication were not sufficient to break this association.

The decrease in dimensions was confirmed by DLS analysis, as the hydrodynamic diameter decreased from 119 ± 3 to 80 ± 1 nm after sonication (**Table 1**).

Table 1 Hydrodynamic size (DLS) and size distribution (AFM & TEM: length, AFM: width) of sonicated and non-sonicated CNC suspensions. The standard deviations are indicated between parentheses.

	Hydrodynamic properties		Size	
	Z (nm)*	*PDI*	*Average length (nm)*	*Height (nm)*
Non-sonicated CNCs	119 (3)	0.20	217 (42)	10 (5)
Sonicated CNCs	80 (1)	0.17	150 (30)	10 (5)

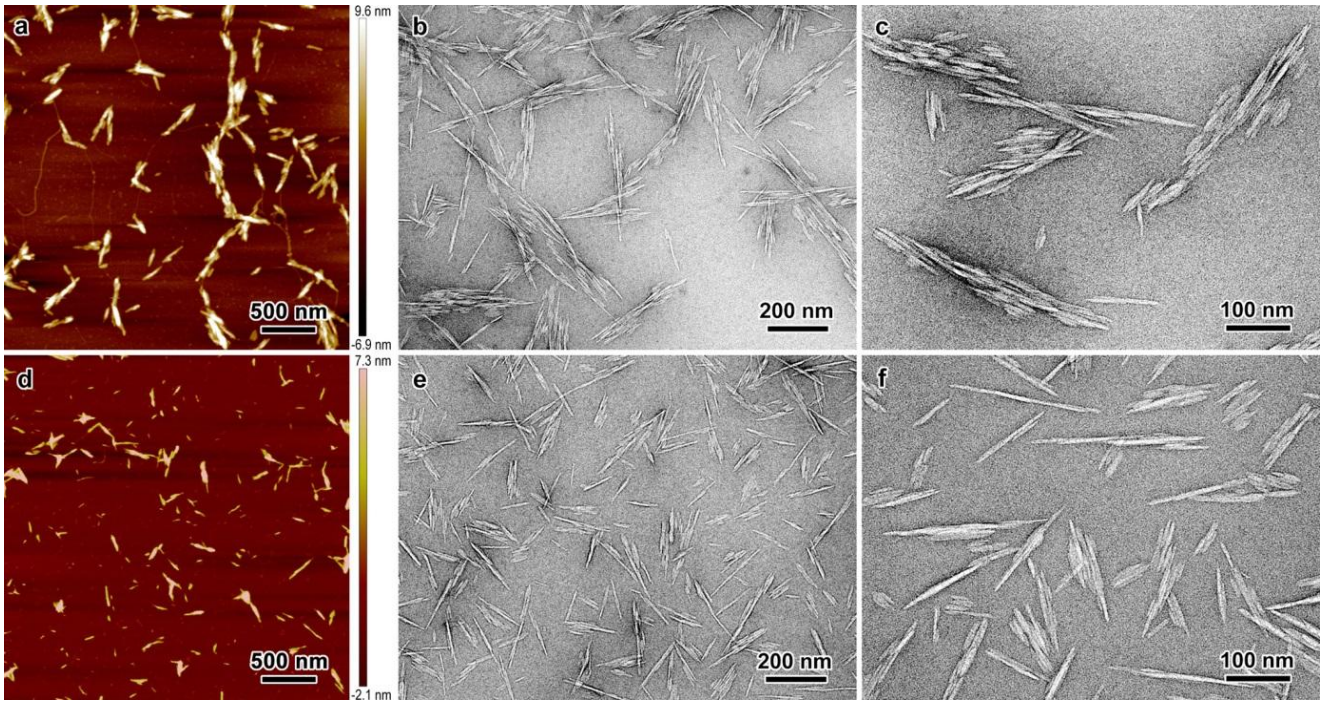

Fig. 2 CNC morphology: a, b, c before sonication; d, e, f after sonication. a and d are AFM images while b, c, e and f are TEM images of negatively stained preparations

2.2. Interparticle distance in static conditions

In order to investigate the effect of sonication on the structural features of the suspensions, analyses at different length scales were performed by SAXS. **Fig. 3** shows the evolution of the average distance between CNCs with the concentration of the suspension. With or without sonication, the general behavior is the same and follows a power law decrease. With increasing concentration, the interparticle distance quickly decreases and reaches a minimum close to 30 nm in the concentration range probed. Both power law fits yield an exponent close to -1/2, which is characteristic of the signal of long cylinders in hexagonal arrangement (Baravian et al., 2010). The elongated shape of the CNCs is thus conserved through the sonication treatment. However, during sonication the spatial distribution of particles is modified and at a given cellulose volume fraction, the interparticle distance is lower after sonication. This effect can be attributed to a sonication-induced scission of the objects that would decrease their aspect ratio. This hypothesis is confirmed by the fact that curve

corresponding to non-sonicated CNCs can be shifted to superimpose with that of the sonicated CNCs by considering a two-fold decrease in the aspect ratio.

The *a*, *b* and *c* characteristic dimensions of CNCs were obtained by plotting the intensity distribution $I(q)$ as a function of scattering vector q and fitting the curves with different form factor models. A parallelepiped model gives the best result, in agreement with already reported SAXS and SANS data (Cherhal et al., 2015; Mao et al., 2017). Dimensions a, b and c extracted from the fitting procedure are 114 x 60 x 4 nm^3 before sonication and 121 x 20 x 5 nm^3 after sonication. However, as already reported (Cherhal et al., 2015), only a very poor accuracy in the length determination can be obtained due to the limited *Q*-range that was probed. More accurate values could be obtained from investigations at much lower *Q*-values. A high polydispersity appears in the calculation of the *b* dimension for non-sonicated CNCs (± 10 nm), which is in line with AFM and TEM images showing objects with large lateral size variations. To stay within confidence limits, it can be concluded that SAXS data show that the sonication treatment induces a decrease in the width of the particles while their height, of the order of the size of elementary crystallites, is unaffected.

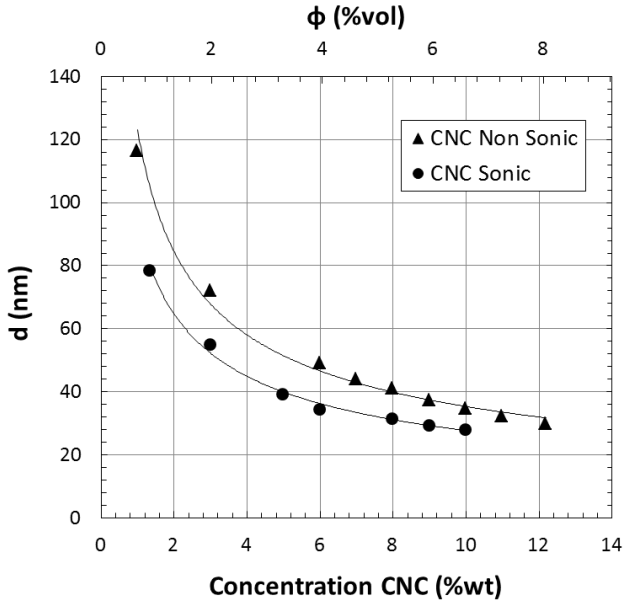

Fig. 3 Average CNC center-to-center interparticle distance d as a function of concentration (in wt%, bottom scale) or volume fraction (ϕ in vol%, top scale) in suspensions at different concentrations, deduced from the Kratky plot ($q^2 \cdot I(q) = f[q]$). CNC were exposed (●) or not exposed (▲) to sonication. Interpolation curves correspond to a power law model. The power law equation is $y = 93x^{-0.53}$ and $y = 123x^{-0.54}$ for sonicated and non-sonicated CNC suspensions, respectively.

2.3. Phase behavior and microstructure after sonication at high concentration

Fig. 4 presents the phase diagrams for sonicated and non-sonicated CNC suspensions. In the first case, a sonicated suspension at a concentration of about 12 wt% has been used for sample preparation, while in the second case the as-delivered 12 wt% non-sonicated batch has been used. The first remarkable feature is that both types of suspensions exhibit a clear phase separation behavior: above a first critical concentration, C_i, biphasic samples are obtained with an upper isotropic phase and a lower birefringent anisotropic one and a fully anisotropic phase is observed above a second critical concentration, C_a (**Fig. 4**). However, the time required to reach equilibrium is strongly ultrasound treatment dependent. Depending on the concentration, it took 5 to 7 days for the non-sonicated suspensions to equilibrate, while for sonicated samples complete phase separation was reached within 20h only. The sonication treatment therefore strongly accelerates the phase separation kinetics.

The critical concentrations were measured in each case as the linear extrapolation in the biphasic gap at 0 and 100 vol % for the critical concentration, C_i and C_a, respectively.

The results show that sonication also has a huge influence on the critical concentration values with C_i ~ 5.8 and 7.5 wt% and C_a ~ 9 and 13.3 wt% for the non-sonicated and sonicated suspensions, respectively. Without sonication, phase separation occurs at lower concentration and the biphasic gap is thinner than with sonication. The biphasic gap in the case of the non-sonicated samples spans over 3.2 wt% (or C_a/ C_i = 1.5*)*, which is an unusually small value compared to what is reported in the literature (Dong and Gray, 1997; Dong et al., 1996). Interestingly, the critical concentrations values reported by Xu et al., in the case of CNCs of the same origin but with samples prepared from the sonication-assisted redispersion in water of a freeze-dried powder, are C_i = 3.5 and C_a =10 wt%, respectively.*i.e.* with a lower C_i value and a higher C_a value than in our non-sonicated case and a much lower C_i and lower C_a than for our sonicated system (Xu et al., 2017b, 2018). This comparison suggests that freeze-drying step could also influence the self-organization properties of this type of CNCs.

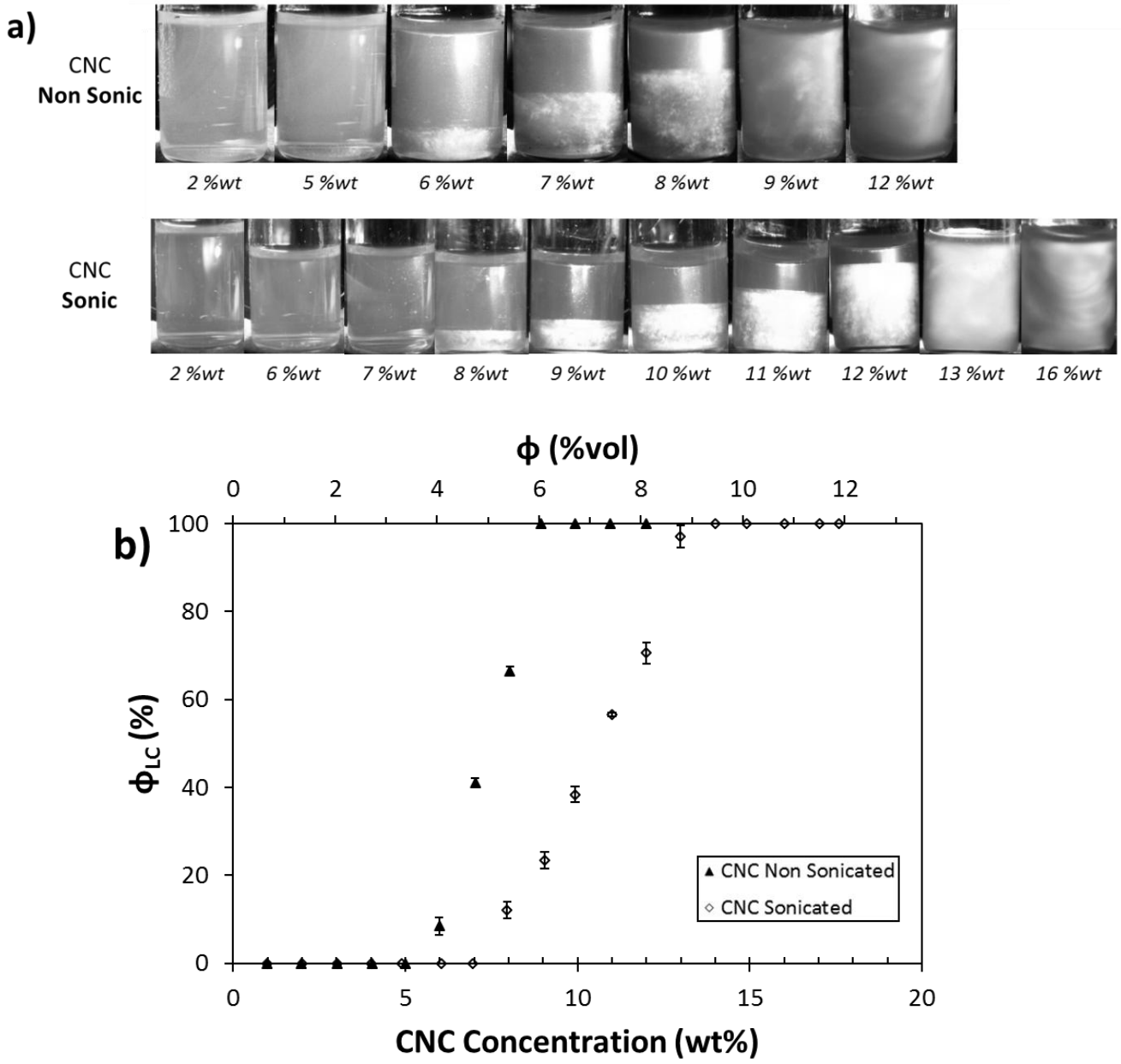

Fig. 4 Phase behavior of aqueous CNC suspensions after equilibration. a) photographs of vials between crossed polars showing the phase separation of CNC suspensions from 1 to 12 wt% (non-sonicated CNCs) and from 1 to 16 wt% (sonicated CNCs). The lower liquid crystalline phase (anisotropic) is white while the upper isotropic phase appears dark. b) Volume fraction of liquid crystalline phase (ϕ_{LC} in vol%) as a function of the solid weight in the CNC suspensions. ▲ and ◇ correspond to non-sonicated and sonicated CNC suspensions, respectively. The error bars represent the standard deviation of the fitted Gaussian peaks.

2.4. Influence of sonication on the rheological behavior

To complete the static and microstructure studies, the rheological behavior of a commercial suspension at 12 wt% was firstly investigated.

Effect of mechanical treatment on highly concentrated CNC suspension rheology

Figure 5 compares the effect of sonication and mechanical homogenization on the rheological behavior of CNC suspensions at 12 wt% after several months of storage at optimum condition in fridge. The non-sonicated initial CNC suspension exhibits a shear-thinning behavior. When the shear rate increases from 0.1 to 1000 s^{-1}, the viscosity drastically decreases from 300 to 0.08 Pa.s, and follows a $v = 49.65\,\dot{\gamma}^{0.06}$ power law . As shown in **Fig. 1**, the suspension in a gel-like form did not flow when the vial was turned upside down.

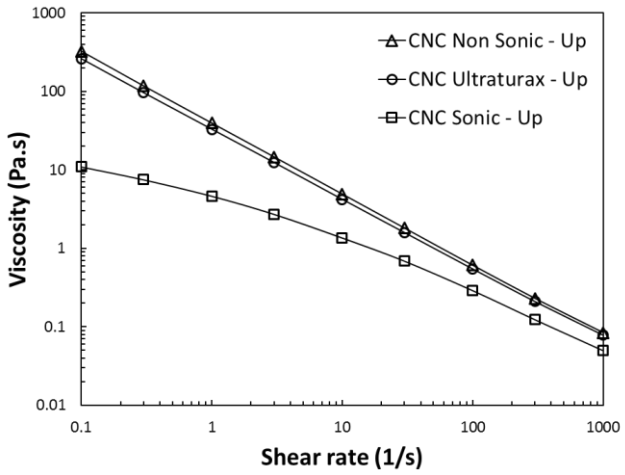

Fig. 5 Flow curves of 12 wt% CNCs suspensions as-received and treated by sonication or by mechanical homogenization.

After a strong mechanical homogenization, the CNC suspension does not exhibit any change in behavior compared to the non-sonicated suspension. However, sonication drastically affects the viscosity, and a more than 10-fold-decrease in viscosity was observed in the low shear-rate region. Accordingly, as shown in **Figure 1,** the sonicated suspension was liquid and flowed when the vial was turned upside down.

Influence of aging time after sonication

Fig. 6 presents the evolution with time of the rheological behavior of a 12 wt% CNC commercial suspension after ultra-sonication treatment. Before sonication, the rheological behavior for the same suspension does not show any time evolution (data not shown). In this figure, two behaviors are identified and separated by a relaxation time-dependent critical shear rate, $\dot{\gamma}_c$. Below this value, a viscosity plateau is obtained. Then, at higher shear rate, a shear-thinning behavior is observed. $\dot{\gamma}_c$ decreases when the relaxation time after sonication increases. In details, just after sonication, the maximum viscosity at low shear rate is close to 0.04 Pa·s and decreases to 0.016 Pa·s at 1000 s^{-1}. During the following hour, the critical shear

rate $\dot{\gamma}_c$ does not change (20 s^{-1}) but the viscosity slightly increases. The characteristic value $\dot{\gamma}_c$, and the general viscosity change after one day of relaxation. As aforementioned, the biphasic domain reaches equilibrium within one day. The viscosity increases because of a reorganization of the CNCs from an isotropic phase to an isotropic/anisotropic biphasic structure. After more than a year of relaxation the viscosity at low shear rate increases to 9 Pa·s and $\dot{\gamma}_c$ decreases to 2.5 s^{-1}.

It has to be noted than despite the described evolution with time, the suspension never comes back to the rheological behavior of the non-sonicated suspension (plotted in **Fig. 5**). Recent work of Beuguel et al. (Beuguel et al., 2018) explain that the use of ultrasonication on CNCs suspension (from spray- and freeze-dried suspensions) will break aggregates and decrease the viscosity. However, according to these authors, no desulfation takes place since this phenomenon would require more energy than generated by sonication. The temporal evolution of the rheological behavior after sonication could be explained by a reorganization of cholesteric domains and/or a possible densification of the CNCs ions double layers (Beck et al., 2010).

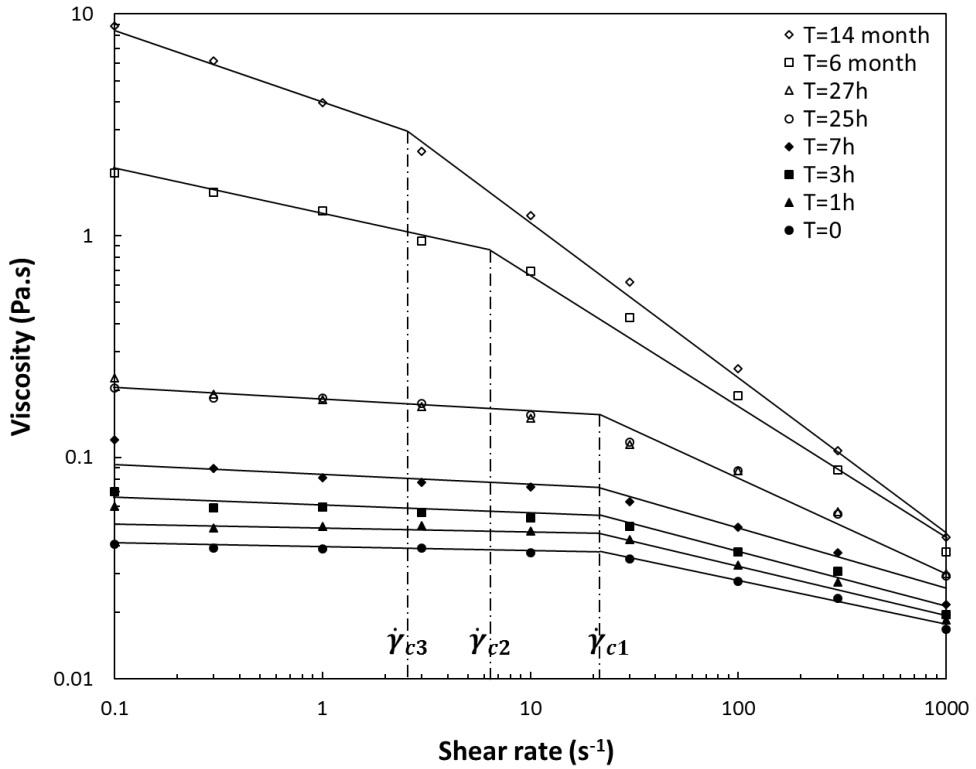

Fig. 6 Flow curve evolution with aging time of sonicated 12 wt% CNCs suspensions. Critical shear rate ($\dot{\gamma}_c$) are indicated in dotted lines, respectively. $\dot{\gamma}_{c1}$, $\dot{\gamma}_{c2}$ and $\dot{\gamma}_{c3}$ are equal to 20, 6 and 2.5 s^{-1}, respectively.

In order to understand the viscoelastic properties and the restructuration after shear rate of both non-sonicated and sonicated 12 wt% suspensions, oscillatory rheology experiments were performed. A constant strain within the linear viscoelastic (LVE) region was applied in order to keep the structural organization unchanged and probe the non-flowing samples. A strong deformation ($\dot{\gamma} = 1000\ s^{-1}$) largely out of the LVE was then applied to break the system and organize CNCs. Then, again, a constant strain within the LVE was applied. G' (elastic modulus in Pa) and G" (viscous modulus in Pa) values quantify respectively the elastic and viscous behavior of the CNC suspension.

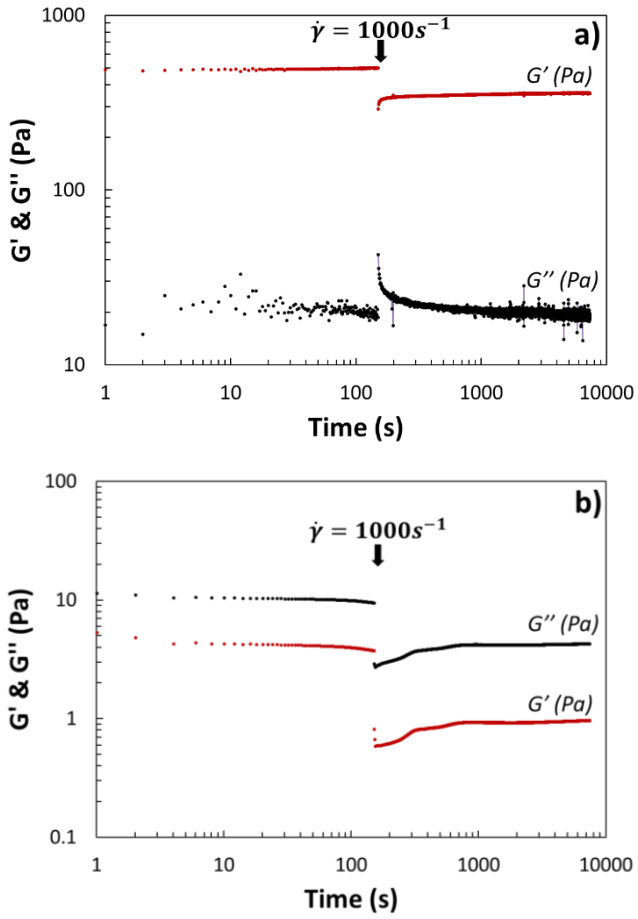

Fig. 7 Evolution of G' (Pa) and G'' (Pa) for non-sonicated (a) and sonicated (aging time 24h) (b) 12 wt% CNC suspensions

With these values, the loss factor $\tan\delta$ can be calculated according to **Equation 1**:

$$(1) \qquad \tan\delta = G''/G' \tag{1}$$

In this equation, if $\tan\delta$ is lower than 1, the elastic modulus (G') dominates and the suspension behaves like a solid. In the opposite case, the viscous modulus (G") controls the system and the material is dominated by a liquid behavior.

The evolution of tan δ is presented in **Fig. 7** and summarized in **Table 2**. In its original state, the loss factor of the non-sonicated 12 wt% commercial suspension is inferior to 1 indicating a dominant elastic behavior. As shown in **Fig. 5**, by applying a strong shear rate the general viscosity decreases from 300 to 0.08 Pa·s. Upon strong deformation, the suspension quickly recovers (200 s) its gel-like behavior with a loss of factor of 0.06.

Table 2 Synthesis of tan δ measurements obtained with G' (elastic modulus in Pa) and G" (viscous modulus in Pa) before and just after applying a shear rate of $1000 s^{-1}$ on 12 wt% CNC suspension

	Before deformation			*After* $\dot{\gamma} = 1000\ s^{-1}$		
	G' (Pa)	G'' (Pa)	**tan δ**	G' (Pa)	G'' (Pa)	**tan δ**
Non-sonicated	490	20	**0.04**	355	20	**0.06**
Sonicated	4	10	**2.5**	1	4	**4**

After sonication, the system is driven by the viscous modulus and presents a loss factor about 2.5. The material is dominated by a liquid behavior. After high shear rate, a loss factor value superior to 1 is preserved.

The rheological properties therefore changes from a gel-like behavior for unsonicated samples to a liquid one for sonicated samples.

2.5. Concentration effect on the CNC rheological behavior

Fig. 8 shows the steady-state flow curves for CNC suspensions in deionized water at different concentrations ranging from 1 to 12 wt%. In complement, **Table 3** presents the power law parameters obtained from fitting regions of the flow curves.

The behavior of CNCs without sonication treatment is shown in **Fig. 8a**. A recent study shows results on the same type of CNCs after redispersion of a freeze-dried powder (Xu et al., 2017b, 2018). While these results are close to our results, all concentrations were not investigated in the publication and the impact of sonication is not evaluated. CNC suspensions behave like near-Newtonian liquids for concentration below 3%wt, as evidenced by a flow index n close to 1 (**Table 3**). By increasing the amount of CNCs in the suspension (4-5 wt%), at low shear rate (<1 s^{-1}) the CNC suspensions exhibit a viscosity plateau close to a zero-shear viscosity plateau and at high shear rate a shear-thinning behavior ($0.9 > n > 0.5$). As shown in **Fig. 4** these concentrations correspond to the fully isotropic region. Then for 6-8%wt CNC suspensions (C_i), corresponding to the appearance of the liquid crystalline phase, the rheological behavior changes to a multi-phase curve as explained by Xu et al. (Xu et al., 2017b). The consistency K starts to increase for a 7 wt% CNC suspension (C_a), which

corresponds to ~40 vol% of liquid crystalline phase. At high shear rate, a significant shear thinning appears with a power law exponent from 0.5 to 0.3 (**Table 3**). The slight shear-thinning at low shear rates may indicate some association between the CNC rods. As previously proposed (Xu et al., 2017b), at higher concentrations, which correspond to the fully anisotropic domain, samples exhibit a strong shear-thinning behavior over the whole range of shear rates probed. The flow index n decreased close to zero for a 12 wt% CNC suspension, which is characteristic of a yield stress fluid. The existence of a closely packed structure locks the rods motion due to an excessive concentration.

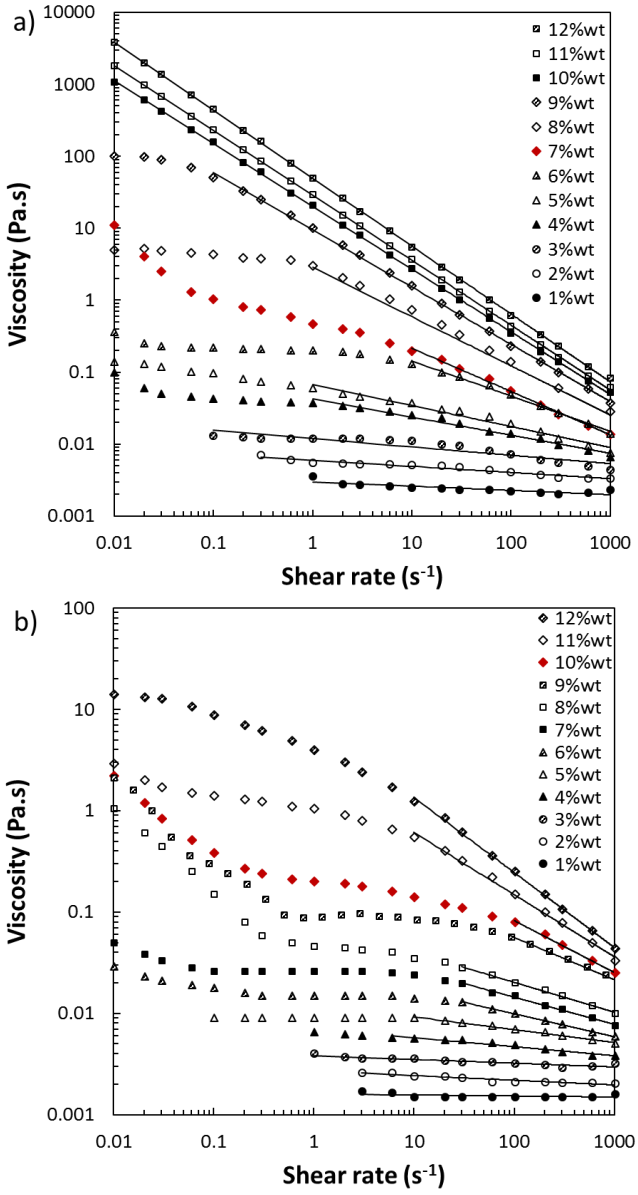

Fig. 8 Investigation on shear rheology of 1-12 wt% CNCs suspension in water: apparent viscosity as function of shear rate for CNC before (a) and after sonication (b). Red diamond corresponds to ϕ_{LC} close to 40 vol%.

Table 3 A list of the power law ($\eta = K \cdot \dot{\gamma}^{n-1}$) parameters obtained from fitting regions of the flow curves in **Fig. 8**.

	vol%	*0.6*	*1.3*	*1.9*	*2.5*	*3.2*	*3.8*	*4.5*	*5.2*	*5.8*	*6.5*	*7.2*	*7.9*
	wt%	*1*	*2*	*3*	*4*	*5*	*6*	*7*	*8*	*9*	*10*	*11*	*12*
CNC Non-sonicated	*K (Pa·s^{-n})*	0.003	0.006	0.023	0.048	0.09	0.053	0.71	2.77	9.35	20.39	28.671	49.65
	n	0.97	0.92	0.89	0.73	0.65	0.48	0.43	0.32	0.21	0.13	0.1	0.06
	Domain	*Isotropic domain*					*Biphasic domain*				*Chiral nematic domain*		
Sonicated CNC	*K (Pa·s^{-n})*	0.002	0.003	0.004	0.007	0.012	0.024	0.045	0.077	0.386	0.515	2.423	4.93
	N	0.97	0.96	0.96	0.92	0.87	0.81	0.75	0.71	0.58	0.57	0.39	0.34
	Domain	*Isotropic domain*							*Biphasic domain*				

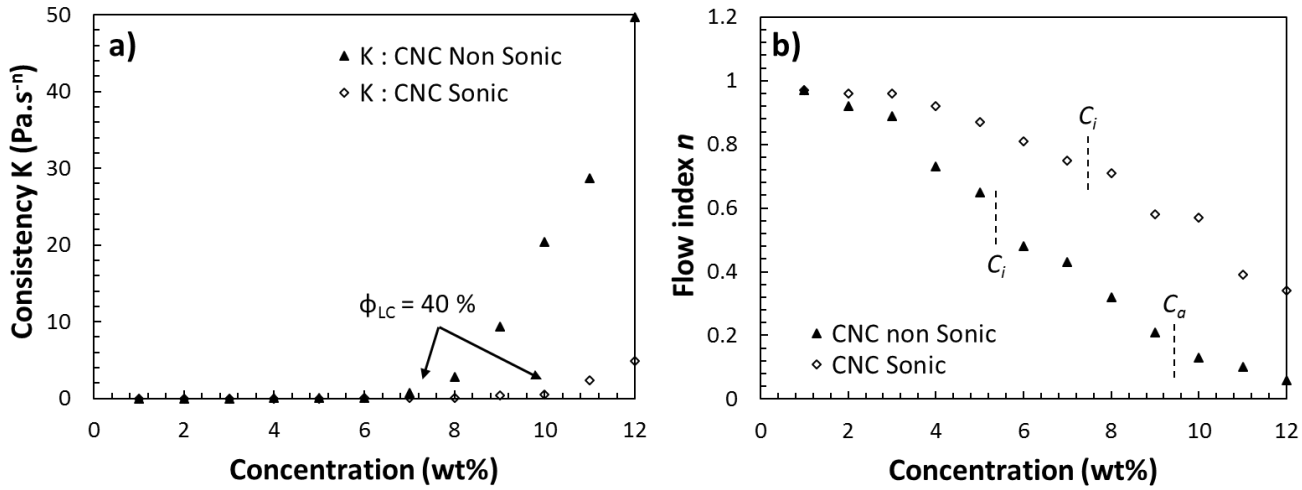

Fig. 9 Plot of the power law parameters for CNCs before and after sonication, referring to **Table 3**: a) consistency K and b) flow index n versus CNCs concentration.

The rheological behavior of sonicated CNC suspensions is shown in **Fig. 8b**. According to **Fig. 4** phase separation starts at C_i = 7.5 wt% and is complete at C_a = 13 wt%. CNC suspensions at 1-4%wt exhibit a near-Newtonian behavior with n between 1 and 0.9 (**Table 3**). In the 5-7 wt% concentration region, at mid shear rate (< 10 s^{-1}), the CNC suspensions exhibit a plateau region and at high shear rate a shear-thinning behavior ($0.75 < n < 0.87$). A slight shear thinning at lower shear rate could be associated to the disruption of the largest chiral nematic domain in smaller chiral nematic domains. Then for concentrations 8, 9 and 10 wt% a three-region behavior was observed, typical of liquid crystalline samples (Bercea and Navard, 2000; Shafiei-Sabet et al., 2012). A low shear rate (< 0.1 s^{-1}), the viscosity decrease has been attributed to the dissociation of the largest chiral nematic domains in smaller chiral nematic domains. Then, for middle range shear rate (1 to 30 s^{-1}), the plateau in viscosity could be associated to the increasing alignment of theses chiral domains in the flow direction. At high shear rate, a significant shear thinning appears and the viscosity decreases: chiral

domains are broken and individual CNCs will be aligned in the flow direction. For higher concentrations (11-12 wt%), the three-regions behavior is not accessible in the shear rate range probed, but a two slopes behavior persists. At $0.1 < \dot{\gamma} < 10$ s^{-1}, the viscosity evolution nearly flat will correspond to organization/orientation of the nematic domains in the shear flow direction. For high shear rate (>10 s^{-1}), the power law parameter n decreases below 0.4 and a shear-thinning behavior is observed. Nematic domains are dissociated and mostly single CNCs would aligned with the flow (Shafiei-Sabet et al., 2012).

An interesting information is emphasized in **Fig. 9a:** the consistency, *K*, drastically increases at 7 wt% for non-sonicated CNCs suspension and at 10 wt% for the sonicated CNCs suspension. In both cases, the volume fraction of liquid crystals deduced from **Fig. 4** is the same with an anisotropic phase volume fraction Φ_{LC} close to 40 vol%. In **Fig. 8**, red diamonds highlight these two specific suspensions at the same Φ_{LC} for which the rheological behaviors of non-sonicated and sonicated CNC suspension are similar. The sonication does not modify the general trend of the rheological behavior of CNC suspensions, but changes the relative concentration when the three rheological behavior regions appear. This observation highlights the fact that the suspension before sonication is not aggregated (in the case of aggregation, the general behavior is totally different (Xu et al., 2017a)) and the parameter that drives the rheological behavior is Φ_{LC}.

In **Fig. 9b**, suspension of sonicated CNCs shows a power law parameter n superior to non-sonicated CNCs which corresponds to a lower shear-thinning behavior. Sonicated CNCs are well dispersed with limited constraints (due to less connection) than non-sonicated CNCs. They will flow easily thanks to minor energy needed to destruct, separate and orientate particles.

2.6. Multi-scale discussion

In **Fig. 4**, the as-received commercial suspension presents a phase separation behavior completed within 5-7 days, whereas longer times of the order of several weeks are usually reported for CNCs prepared from wood. This behavior proves the absence of aggregates, whose presence would not allow the self-organization to occur.

By comparing **Fig. 4 and 8** for both systems, it can be concluded that the rheological results present a three-regions behavior in line with the three domains observed in the phase diagram. In the fully isotropic domain, both systems present a near Newtonian nature. A plateau region appears for low shear rate. It is the beginning of the shear-thinning properties. In the biphasic domain, both systems present three rheological behavior regions as described in the literature (Ureña-Benavides et al., 2011). In the fully anisotropic region, the non-sonicated suspension is totally shear-thinning, with a shear thinning index n close to zero characteristic of a gel-like behavior.

This behavior might be attributed to the presence of aggregates in the CNC suspension before sonication. Some recent works have explored this hypothesis (Ureña-Benavides et al., 2011; Xu et al., 2017a, 2017b, 2018) but the authors used re-suspended freeze-dried CNCs in their studies. This process induced the formation of aggregates. In our case, however, CNC suspensions have never been freeze-dried and did not contain aggregates. As shown by AFM, TEM and DLS data (**Table 1** and **Fig. 2**) non-sonicated suspensions are composed of stable particles composed of the association of tenths of elementary crystallites into elongated bundles. Then, the gel behavior in the non sonicated CNC suspensions at high concentration, studied in this work would result from repulsive interactions of CNC particles were particles dynamics is arrested as described by Xu et al. (Xu et al., 2018). TEM, AFM, DLS and SAXS results concur to show that sonication induces a scission of the initial elongated elementary crystallites bundles into shorter and thinner objects composed of a smaller number of elementary subunits. In other words, one of the main effects of sonication is a significant decrease of the aspect ratio of the particles. Consistently and in agreement with Onsager's theory that shows that critical concentrations are inversely proportional to the aspect ratio of the particles, the phase separation behavior is shifted to higher concentrations for sonicated suspensions. However, it has to be noted that there might be other modifications induced by sonication. Beck and coworkers reported that a bound-water layer or a gel layer of sulfated oligosaccharides surrounds CNCs. They suggest that this layer contains ions originating from the hydrolysis process that might be ejected during the sonication, resulting in a larger electrical double layer and weaker chiral interactions (Beck et al., 2010, 2012). Such a mechanism would also lead to a shift towards higher concentration of the critical liquid crystalline boundaries.

The drastic difference in viscosity at high concentration and low shear rate illustrated in **Fig. 1,** can also be ascribed to this aspect ratio variation. Indeed, non-sonicated high aspect ratio

particles logically tend to form a connected gel-like structure whereas lower aspect ratio sonicated CNCs suspensions flow due to the absence of physical interactions between the objects. As far as the rheological behavior is concerned, both non-sonicated and sonicated suspensions behave similarly and exhibit the standard rheological behavior of CNCs (Shafiei-Sabet et al., 2012; Ureña-Benavides et al., 2011) (**Fig. 8**). However, the different critical concentrations are shifted to higher values after sonication (e.g. the typical behavior of biphasic liquid crystalline suspensions appears at 7 wt% before sonication and at 10 wt% after sonication). These suspensions did not show any aggregated objects behavior and the effect of sonication is irreversible on CNCs even if some temporal variations were observed (**Fig. 6**).

Conclusions

The microstructure and the rheological behavior of a highly concentrated suspension of cellulose nanocrystals from University of Maine have been studied, and the behavior of never freeze-dried non-sonicated and sonicated suspensions were compared. The sonication treatment results in morphological modifications and induces a decrease of the suspension viscosity. Both suspensions present three-region phase diagrams, which correspond to three different microstructural transitions: isotropic region, biphasic region (coexistence of isotropic and chiral nematic form) and a birefringent gel. Sonication increases the critical concentrations C_i and C_a and the width of the biphasic gap and also affects the general viscosity of each concentration. At 12 wt%, the suspension is gel-like before sonication and totally turns to a liquid form after sonication treatment. The microstructure, and in particular the inter-particular distance d, is changed by this treatment. TEM, AFM, DLS and SAXS analyses consistently show that sonication induces a decrease of the aspect ratio of the particles, which can explain the observed self-organization and rheological behaviors and data rule out the presence of aggregates in the initial suspension.

The viscosity profile of the non-sonicated CNC suspensions shows a single shear-thinning behavior over the whole range of shear rates for concentrations higher than 9 wt%. By decreasing the concentration, a three-region behavior appears followed by a Newtonian plateau for concentrations under 3 %wt. After sonication, at high concentration, the system is stable again but presents a higher decrease of viscosity and a higher shear-thinning index. At intermediate concentrations, a notable three region plateau typical of liquid-crystal has been

548 emphasis. Then at concentrations lower than 4 wt%, the rheological behavior of the
549 suspensions is Newtonian.
550 In this paper we have described the behavior of a commercial CNC suspension before and
551 after sonication at high concentration. This suspension is used in many industrial applications
552 and this study will open new opportunities for applications involving nanocrystalline cellulose
553 like shear-thinning polymer, injectable or pump-ability liquid and matrices reinforcement.
554
555

Acknowledgment

This work has been partially supported by the PolyNat Carnot Institute (Investissements d'Avenir - grant agreement n°ANR-11-CARN-007-01). This research has been possible thanks to the facilities of the TekLiCell platform funded by the Région Rhône-Alpes (ERDF: European regional development fund). We thank the NanoBio-ICMG platform (Grenoble, FR 2607) for granting access to the Electron Microscopy facility. This work benefitted from SasView software 4.0.1, originally developed by the DANSE project under NSF award DMR-0520547 (SasView, http://www.sasview.org/). The Laboratoire Rhéologie et Procédés is part of the LabEx Tec21 (Investissements d'Avenir – grant agreement ANR-11-LABX-0033). All laboratories are part of Institut Carnot PolyNat (Investissements d'Avenir – grant agreement ANR-11-CARN-030-01) and the Glyco@Alps program (Initiative d'Excellence – grant agreement ANR-15-IDEX-02). We gratefully acknowledge the ESRF for the beam time allocation (proposal SC 4177).

References

Abitbol, T., Kam, D., Levi-Kalisman, Y., Gray, D.G., and Shoseyov, O. (2018). Surface Charge Influence on the Phase Separation and Viscosity of Cellulose Nanocrystals. Langmuir *34*, 3925–3933.

Araki, J., and Kuga, S. (2001). Effect of Trace Electrolyte on Liquid Crystal Type of Cellulose Microcrystals. Langmuir *17*, 4493–4496.

Azzam, F., Heux, L., and Jean, B. (2016). Adjustment of the chiral nematic phase properties of cellulose nanocrystals by polymer grafting. Langmuir *32*, 4305–4312.

Baravian, C., Michot, L.J., Paineau, E., Bihannic, I., Davidson, P., Impéror-Clerc, M., Belamie, E., and Levitz, P. (2010). An effective geometrical approach to the structure of colloidal suspensions of very anisometric particles. EPL Europhys. Lett. *90*, 36005.

Beck, S., Bouchard, J., and Berry, R. (2010). Controlling the Reflection Wavelength of Iridescent Solid Films of Nanocrystalline Cellulose. Biomacromolecules *12*, 167–172.

Beck, S., Bouchard, J., and Berry, R. (2012). Dispersibility in Water of Dried Nanocrystalline Cellulose. Biomacromolecules *13*, 1486–1494.

Beck-Candanedo, S., Roman, M., and Gray, D.G. (2005). Effect of Reaction Conditions on the Properties and Behavior of Wood Cellulose Nanocrystal Suspensions. Biomacromolecules *6*, 1048–1054.

Bercea, M., and Navard, P. (2000). Shear Dynamics of Aqueous Suspensions of Cellulose Whiskers. Macromolecules *33*, 6011–6016.

Beuguel, Q., Tavares, J.R., Carreau, P.J., and Heuzey, M.-C. (2018). Ultrasonication of spray- and freeze-dried cellulose nanocrystals in water. J. Colloid Interface Sci. *516*, 23–33.

Bras, J., Viet, D., Bruzzese, C., and Dufresne, A. (2011). Correlation between stiffness of sheets prepared from cellulose whiskers and nanoparticles dimensions. Carbohydr. Polym. *84*, 211–215.

Chauve, G., Fraschini, C., and Jean, B. (2014). Separation of cellulose nanocrystals. Handb. Green Mater. Process. Technol. Prop. Appl. World Sci Pub Co Lond. 73–87.

Cherhal, F., Cousin, F., and Capron, I. (2015). Influence of Charge Density and Ionic Strength on the Aggregation Process of Cellulose Nanocrystals in Aqueous Suspension, as Revealed by Small-Angle Neutron Scattering. Langmuir *31*, 5596–5602.

Csiszar, E., Kalic, P., Kobol, A., and Ferreira, E. de P. (2016). The effect of low frequency ultrasound on the production and properties of nanocrystalline cellulose suspensions and films. Ultrason. Sonochem. *31*, 473–480.

Dong, X.M., and Gray, D.G. (1997). Effect of Counterions on Ordered Phase Formation in Suspensions of Charged Rodlike Cellulose Crystallites. Langmuir *13*, 2404–2409.

605 Dong, X.M., Kimura, T., Revol, J.-F., and Gray, D.G. (1996). Effects of Ionic Strength on the
606 Isotropic−Chiral Nematic Phase Transition of Suspensions of Cellulose Crystallites. Langmuir
607 *12*, 2076–2082.

608 Dong, X.M., Revol, J.-F., and Gray, D.G. (1998). Effect of microcrystallite preparation
609 conditions on the formation of colloid crystals of cellulose. Cellulose *5*, 19–32.

610 Ebeling, T., Paillet, M., Borsali, R., Diat, O., Dufresne, A., Cavaille, J.Y., Chanzy, H., and others
611 (1999). Shear-induced orientation phenomena in suspensions of cellulose microcrystals,
612 revealed by small angle X-ray scattering. Langmuir *15*, 6123–6126.

613 Elazzouzi-Hafraoui, S., Nishiyama, Y., Putaux, J.-L., Heux, L., Dubreuil, F., and Rochas, C.
614 (2008). The Shape and Size Distribution of Crystalline Nanoparticles Prepared by Acid
615 Hydrolysis of Native Cellulose. Biomacromolecules *9*, 57–65.

616 García, A., Gandini, A., Labidi, J., Belgacem, N., and Bras, J. (2016). Industrial and crop
617 wastes: A new source for nanocellulose biorefinery. Ind. Crops Prod. *93*, 26–38.

618 Gicquel, E. (2017). Development of stimuli-responsive cellulose nanocrystals hydrogels for
619 smart applications. Ph.D. Thesis. Grenoble Alpes University.

620 Gicquel, E., Martin, C., Yanez, J.G., and Bras, J. (2017). Cellulose nanocrystals as new bio-
621 based coating layer for improving fiber-based mechanical and barrier properties. J. Mater.
622 Sci. *52*, 3048–3061.

623 Habibi, Y., Lucia, L.A., and Rojas, O.J. (2010). Cellulose Nanocrystals: Chemistry, Self-
624 Assembly, and Applications. Chem. Rev. *110*, 3479–3500.

625 Hamley, I.W. (2010). Liquid crystal phase formation by biopolymers. Soft Matter *6*, 1863–
626 1871.

627 Hoeng, F., Bras, J., Gicquel, E., Krosnicki, G., and Denneulin, A. (2017). Inkjet printing of
628 nanocellulose–silver ink onto nanocellulose coated cardboard. RSC Adv. *7*, 15372–15381.

629 Honorato-Rios, C., Lehr, C., Schütz, C., Sanctuary, R., Osipov, M.A., Baller, J., and Lagerwall,
630 J.P.F. (2018). Fractionation of cellulose nanocrystals: enhancing liquid crystal ordering
631 without promoting gelation. NPG Asia Mater. *10*, 455.

632 Jorfi, M., and Foster, E.J. (2015). Recent advances in nanocellulose for biomedical
633 applications. J. Appl. Polym. Sci. *132*.

634 Lagerwall, J.P., Schütz, C., Salajkova, M., Noh, J., Park, J.H., Scalia, G., and Bergström, L.
635 (2014). Cellulose nanocrystal-based materials: from liquid crystal self-assembly and glass
636 formation to multifunctional thin films. NPG Asia Mater. *6*, e80.

637 Lee, S.-D. (1987). A numerical investigation of nematic ordering based on a simple hard-rod
638 model. J. Chem. Phys. *87*, 4972–4974.

639 Lin, N., and Dufresne, A. (2014). Nanocellulose in biomedicine: current status and future
640 prospect. Eur. Polym. J. *59*, 302–325.

641 Liu, D., Chen, X., Yue, Y., Chen, M., and Wu, Q. (2011a). Structure and rheology of
642 nanocrystalline cellulose. Carbohydr. Polym. *84*, 316–322.

643 Liu, H., Wang, D., Song, Z., and Shang, S. (2011b). Preparation of silver nanoparticles on
644 cellulose nanocrystals and the application in electrochemical detection of DNA hybridization.
645 Cellulose *18*, 67–74.

646 Lu, A., Hemraz, U., Khalili, Z., and Boluk, Y. (2014). Unique viscoelastic behaviors of colloidal
647 nanocrystalline cellulose aqueous suspensions. Cellulose *21*, 1239–1250.

648 Mao, Y., Liu, K., Zhan, C., Geng, L., Chu, B., and Hsiao, B.S. (2017). Characterization of
649 Nanocellulose Using Small-Angle Neutron, X-ray, and Dynamic Light Scattering Techniques. J.
650 Phys. Chem. B *121*, 1340–1351.

651 Marchessault, R.H., Morehead, F.F., and Koch, M.J. (1961). Some hydrodynamic properties
652 of neutral suspensions of cellulose crystallites as related to size and shape. J. Colloid Sci. *16*,
653 327–344.

654 Mariano, M., El Kissi, N., and Dufresne, A. (2014). Cellulose nanocrystals and related
655 nanocomposites: Review of some properties and challenges. J. Polym. Sci. Part B Polym.
656 Phys. *52*, 791–806.

657 Oksman, K., Mathew, A.P., Bismarck, A., Rojas, O., and Sain, M. (2014). Handbook of Green
658 Materials: Processing Technologies, Properties and Applications: Volume 5 (World Scientific).

659 Onsager, L. (1949). The Effects of Shape on the Interaction of Colloidal Particles. Ann. N. Y.
660 Acad. Sci. *51*, 627–659.

661 Orts, W.J., Godbout, L., Marchessault, R.H., and Revol, J.-F. (1998). Enhanced Ordering of
662 Liquid Crystalline Suspensions of Cellulose Microfibrils: A Small Angle Neutron Scattering
663 Study. Macromolecules *31*, 5717–5725.

664 Rånby, B.G. (1951). Fibrous macromolecular systems. Cellulose and muscle. The colloidal
665 properties of cellulose micelles. Discuss. Faraday Soc. *11*, 158–164.

666 Reid, M.S., Villalobos, M., and Cranston, E.D. (2017). Benchmarking Cellulose Nanocrystals:
667 From the Laboratory to Industrial Production. Langmuir *33*, 1583–1598.

668 Revol, J.-F., Bradford, H., Giasson, J., Marchessault, R.H., and Gray, D.G. (1992). Helicoidal
669 self-ordering of cellulose microfibrils in aqueous suspension. Int. J. Biol. Macromol. *14*, 170–
670 172.

671 Revol, J.-F., Godbout, L., Dong, X.-M., Gray, D.G., Chanzy, H., and Maret, G. (1994). Chiral
672 nematic suspensions of cellulose crystallites; phase separation and magnetic field
673 orientation. Liq. Cryst. *16*, 127–134.

674 Schütz, C., Agthe, M., Fall, A.B., Gordeyeva, K., Guccini, V., Salajková, M., Plivelic, T.S.,
675 Lagerwall, J.P.F., Salazar-Alvarez, G., and Bergström, L. (2015). Rod Packing in Chiral Nematic
676 Cellulose Nanocrystal Dispersions Studied by Small-Angle X-ray Scattering and Laser
677 Diffraction. Langmuir *31*, 6507–6513.

678 Shafiei-Sabet, S., Hamad, W.Y., and Hatzikiriakos, S.G. (2012). Rheology of nanocrystalline
679 cellulose aqueous suspensions. Langmuir ACS J. Surf. Colloids *28*, 17124–17133.

680 Shafiei-Sabet, S., Hamad, W.Y., and Hatzikiriakos, S.G. (2014). Ionic strength effects on the
681 microstructure and shear rheology of cellulose nanocrystal suspensions. Cellulose *21*, 3347–
682 3359.

683 Siqueira, G., Bras, J., and Dufresne, A. (2010). Cellulosic Bionanocomposites: A Review of
684 Preparation, Properties and Applications. Polymers *2*, 728–765.

685 Sunasee, R., Hemraz, U.D., and Ckless, K. (2016). Cellulose nanocrystals: a versatile
686 nanoplatform for emerging biomedical applications. Expert Opin. Drug Deliv. *13*, 1243–1256.

687 Tang, J., Sisler, J., Grishkewich, N., and Tam, K.C. (2017). Functionalization of cellulose
688 nanocrystals for advanced applications. J. Colloid Interface Sci. *494*, 397–409.

689 Ureña-Benavides, E.E., Ao, G., Davis, V.A., and Kitchens, C.L. (2011). Rheology and Phase
690 Behavior of Lyotropic Cellulose Nanocrystal Suspensions. Macromolecules *44*, 8990–8998.

691 Watson, J.D. (1954). The structure of tobacco mosaic virus: I. X-ray evidence of a helical
692 arrangement of sub-units around the longitudinal axis. Biochim. Biophys. Acta *13*, 10–19.

693 Xu, H.-N., Tang, Y.-Y., and Ouyang, X.-K. (2017a). Shear-Induced Breakup of Cellulose
694 Nanocrystal Aggregates. Langmuir *33*, 235–242.

695 Xu, Y., Atrens, A.D., and Stokes, J.R. (2017b). Rheology and microstructure of aqueous
696 suspensions of nanocrystalline cellulose rods. J. Colloid Interface Sci. *496*, 130–140.

697 Xu, Y., Atrens, A.D., and Stokes, J.R. (2018). “Liquid, gel and soft glass” phase transitions and
698 rheology of nanocrystalline cellulose suspensions as a function of concentration and salinity.
699 Soft Matter *14*, 1953–1963.

700 Zhang, J., Albelda, M.T., Liu, Y., and Canary, J.W. (2005). Chiral nanotechnology. Chirality *17*,
701 404–420.

702